Biochemical and Biophysical Research Communications **272,** 29–35 (2000)
doi:10.1006/bbrc.2000.2712, available online at http://www.idealibrary.com on IDEAL®

Zinc–Histidine as Nucleation Centers for Growth of ZnS Nanocrystals

Richard Kho, Liem Nguyen, Claudia L. Torres-Martínez, and Rajesh K. Mehra[1]
Environmental Toxicology Graduate Program, Department of Neuroscience, University of California, Riverside, California 92521

Received March 23, 2000

Histidine is a chelator of zinc, most notably in zinc-finger proteins (zinc coordinated by cysteine and histidine) and in hyperaccumulator plants. Sulfide incorporation into molecules containing metal–cysteinyl complexes has been shown to occur *in vivo* in certain yeasts, leading to enhanced metal tolerance. Demonstrated here for the first time is incorporation of sulfide into zinc–histidine, resulting in histidine–ZnS nanocrystals (NCs) having unique optical properties. Sulfide complexation occurred optimally at alkaline pH into zinc-(histidine)$_2$ species, and UV/Vis absorption maxima were red-shifted as increasing sulfide addition occurred. Intermediate sulfide concentrations led to multiple, thermodynamically preferred NC species within a sample. Fluorescence of histidine–ZnS NCs was greater than ZnS prepared previously with cysteinyl peptides. Transmission electron microscopy and selected-area electron diffraction indicated hexagonal ZnS crystals having an average size of 4.2 nm. A photocatalytic application of histidine–ZnS NCs was shown by efficient degradation of *p*-nitrophenol and paraquat in the presence of UV irradiation. © 2000 Academic Press

Key Words: **histidine; zinc; ZnS; nanocrystal; size-exclusion chromatography; fluorescence; photocatalysis.**

L-Histidine is a nonessential amino acid biosynthesized from ribose phosphate (1). Although nonessential by definition, histidine has numerous essential roles including maintenance of redox status (2) and formation of immuno- and neuropeptides such as histamine and carnosine (3), respectively. Perhaps a more significant role of histidine involves its metal-chelating properties. Zinc-finger proteins, in which zinc is coordinated by cysteine and histidine, are transcription factors critical for regulation of cellular growth and metabolism (4, 5).

The chelation of metals by biomolecules, under certain circumstances, serves as a defense mechanism employed by some species to withstand exposure to toxic metal ions. In the so-called "hyperaccumulator" plants, for example, histidine is known to play a central role in chelation and transport of such metals as zinc, nickel, cobalt and copper leading to metal tolerance (6–8). And in plants and certain yeasts, the cysteinyl peptides glutathione (GSH) and phytochelatins (PCs) were shown to bind cadmium ions, forming Cd-GSH and Cd-PC complexes, respectively (9, 10). An interesting phenomenon occurred in cadmium exposed *Schizosaccharomyces pombe* and *Candida glabrata*. In response to cadmium exposure, these yeasts produced peptide-coated CdS semiconductor nanocrystallites (NCs) having size-quantization effects (10, 11). Considerable evidence exists to show that CdS NCs were synthesized first by metal chelation via GSH or PCs, and then incorporation of labile sulfide (10–12). The latter step, leading to the formation of nanocrystallites, was thought to enhance tolerance by increasing cadmium stability in a non-toxic form. By utilizing this biomolecule-mediated metal chelation approach, our laboratory has shown that the *in vivo* synthesis of semiconductor NCs can be simulated *in vitro*, with greater product yields and controlled optical properties (13–16).

Having demonstrated sulfide incorporation into zinc-cysteine centers, it was postulated that zinc-histidine would also act as matrices for incorporation of sulfide. We report here for the first time that zinc-histidine complexes act as nucleation centers for sulfide incorporation, leading to ZnS nanocrystal growth. The reaction conditions leading to various histidine-ZnS NC species are described. The incorporation of sulfide into preformed zinc-histidine complexes to form NCs has multiple implications. Like the aforementioned yeasts that produced NCs via Cd-GSH or Cd-PC complexes, it does not escape one's imagination that in some organ-

[1] To whom correspondence should be addressed at Environmental Toxicology Graduate Program, 5419 Alfred M. Boyce Hall, University of California, Riverside, CA 92521. Fax: (909) 787-3087. E-mail: rajesh.mehra@ucr.edu.

0006-291X/00 $35.00

isms, NC synthesis *in vivo* might be occurring at metal-histidine nuclei as a mechanism of metal tolerance. Furthermore, the potential application of thus formed NCs in biological labeling may be advanced as a result of the unusual optical properties of histidine-ZnS NCs, such as multiple excitation maxima and increased fluorescence, combined with the high aqueous solubility (17). Also, light absorption and charge transfer through the imidazole ring of histidine may improve the utility of ZnS NCs in photocatalytic applications; photo-redox degradation of *p*-nitrophenol (a model pollutant) and paraquat (a dye) by histidine-ZnS NCs is demonstrated.

MATERIALS AND METHODS

Sodium sulfide, zinc sulfate, imidazole, Tris (hydroxymethyl) aminomethane and other routine chemicals were purchased from Fisher Scientific. L-Histidine, and histamine dihydrochloride were purchased from Alexis. Sephadex G-25 and G-50, fine grade, were procured from Sigma. High quality deionized water (Nanopure, Inc.) was used in all experiments.

A general procedure for synthesis of histidine-capped ZnS NCs was as follows. A 0.25 M solution of histidine was prepared in degassed/N_2 saturated 1 M Tris, pH 10.6. To this solution, 1 M $ZnSO_4$ (in 0.01 N HCl) was added to reach a zinc concentration of 0.125 M, resulting in a molar ratio of 2:1 histidine-to-zinc. To 2 mL aliquots of the above solution, various volumes of sulfide as 1 M Na_2S were added with vortexing to achieve sulfide/Zn ratios of 0.25, 0.5, 0.75, 1.0, 1.5, or 2.0. (Samples will be referenced according to this sulfide/Zn ratio throughout the manuscript). The order in which these reactions take place is critical for synthesis of nanometer-sized particles; i.e., zinc-histidine complex must be formed prior to sulfide addition. The samples were sealed and incubated for 60 min at room temperature. For the purposes of comparing the buffer medium, samples were prepared in water (adjusted to pH 11 with 1.5 M NaOH) instead of 1 M Tris, and pH of the solution following $ZnSO_4$ titration was also adjusted to pH 11 using NaOH.

For isolation of products with greater sample homogeneity, a size-exclusion chromatography procedure was used (14). Samples prepared in Tris buffer were size-fractionated through a medium sized column (1.6 cm $\times$ 30 cm) containing Sephadex G-25 equilibrated with 10 mM Tris, pH 10; the load volume and fraction volume were 2 mL and 1 mL, respectively. Histidine-ZnS NCs prepared in water, meanwhile, were fractionated in a narrower column (0.55 cm $\times$ 20 cm) having a Sephadex G-50 matrix equilibrated with 1 mM NaOH, pH 10, with 0.5 mL load and 0.25 mL fraction volumes.

UV/Vis absorption spectra were recorded on a Perkin-Elmer double-beam spectrophotometer (Lambda 3) controlled by PECSS software. Steady-state, room temperature excitation and emission spectra were recorded on a Perkin-Elmer LS50B spectrofluorometer run by FLDM software. Unless noted, emission spectra were recorded using an excitation wavelength of 290 nm, using bandpass filters at appropriate wavelengths to minimize scattering and secondary emissions. High-resolution transmission electron microscopy (hrTEM) and selected-area electron diffraction (SAED) were performed on a Phillips CM300 transmission electron microscope operating at 300 kV. The samples were appropriately diluted and deposited onto 300-mesh copper grids coated with an ultra-thin carbon support film. The grids were allowed to air dry at room temperature. Electron micrograph images were analyzed using Adobe Photoshop 5.0 and Scion Image software (Scion Corporation), and average nanocrystal size was estimated by measuring across lattice planes of multiple, high-resolution crystal images.

Degradation of *p*-nitrophenol (pNP) was performed to study the photocatalytic properties of thus formed histidine-ZnS NCs. Solutions of NCs and pNP were mixed in 10 mM Tris buffer of varying pH in a septum-sealed quartz cuvette (1 cm pathlength), to form a reaction volume of 2 mL. The ratio of ZnS NC to pNP was 10:1. Photocatalytic degradation was initiated by placing the cuvette 1 cm from an 8-W, shortwave UV lamp (Glo-Mark Systems, Inc.; 254–320 nm, 41 $\pm$ 1 μEinstein/m^2/s approximate photon flux). pNP concentrations were determined by recording absorbance at 405 nm at regular time intervals. Irradiation was terminated when pNP remaining was less than 10%. Photoreduction of paraquat was performed as described previously (13). In brief, irradiation with the shortwave UV lamp was performed for 30 min on samples containing only paraquat, or samples containing paraquat and histidine-ZnS NCs. UV/Vis absorbance spectra were recorded prior to and following irradiation.

RESULTS AND DISCUSSION

Spectroscopic determination of sulfide incorporation into zinc-histidine. For incorporation of sulfide to occur, suitable zinc-histidine matrices must be formed. The chelation of zinc by histidine was optimal above the pK_a of the imidazole group (pK_a = 6.5), suggesting a major involvement of the imidazole nitrogen in zinc coordination. At too high a pH (>12), white precipitates were formed upon zinc titration, suggesting the formation of zinc hydroxide. Using 1 M Tris (pH 10.7) as the buffer, a suitable pH was maintained for formation of zinc-(histidine)$_2$ species. This 2:1 ratio was found to be optimal for subsequent incorporation of sulfide.

The incorporation of sulfide into the preformed zinc-histidine complexes was monitored via UV/Vis absorption spectroscopy. Zinc-histidine complex, at twice excess histidine, shows an absorption λ_{max} of 231 nm (Fig. 1a). As increasing concentrations of sulfide are titrated into zinc-histidine complexes, the absorption maxima shift to higher wavelengths in the range of 260 to 305 nm, and are indicative of ZnS nanocrystal formation (Fig. 1a). The UV/Vis spectrum of 1.0 sulfide/Zn sample showed sharper excitonic transitions with two absorption shoulders having maxima around 265 nm (~4.7 eV, bandgap energy) and 285 nm (~4.35 eV), while the other samples had relatively broad absorption bands. All of these bandgap energies are considerably blue-shifted as compared to the bandgap energy of bulk ZnS (~3.6 eV), demonstrating quantum confinement of these histidine-ZnS materials (18).

The red-shifting of the absorption maxima with increasing initial sulfide was expected (13, 15) and may be due to a size-series of NC product; in general, larger NCs have red-shifted absorption maxima (18). UV/Vis spectra of the peak fractions eluting from a column (1.6 cm $\times$ 30 cm) of Sephadex G-25 showed that the individual fractions had significant overlap of absorption maxima, suggesting a relatively modest size distribution (Fig. 1b). Room-temperature fluorescence of these samples further suggested similar optical properties, as fluorescence maxima were also nearly overlapping (Fig. 1c). The fluorescence intensities of these ZnS NCs were considerably higher than observed previously for

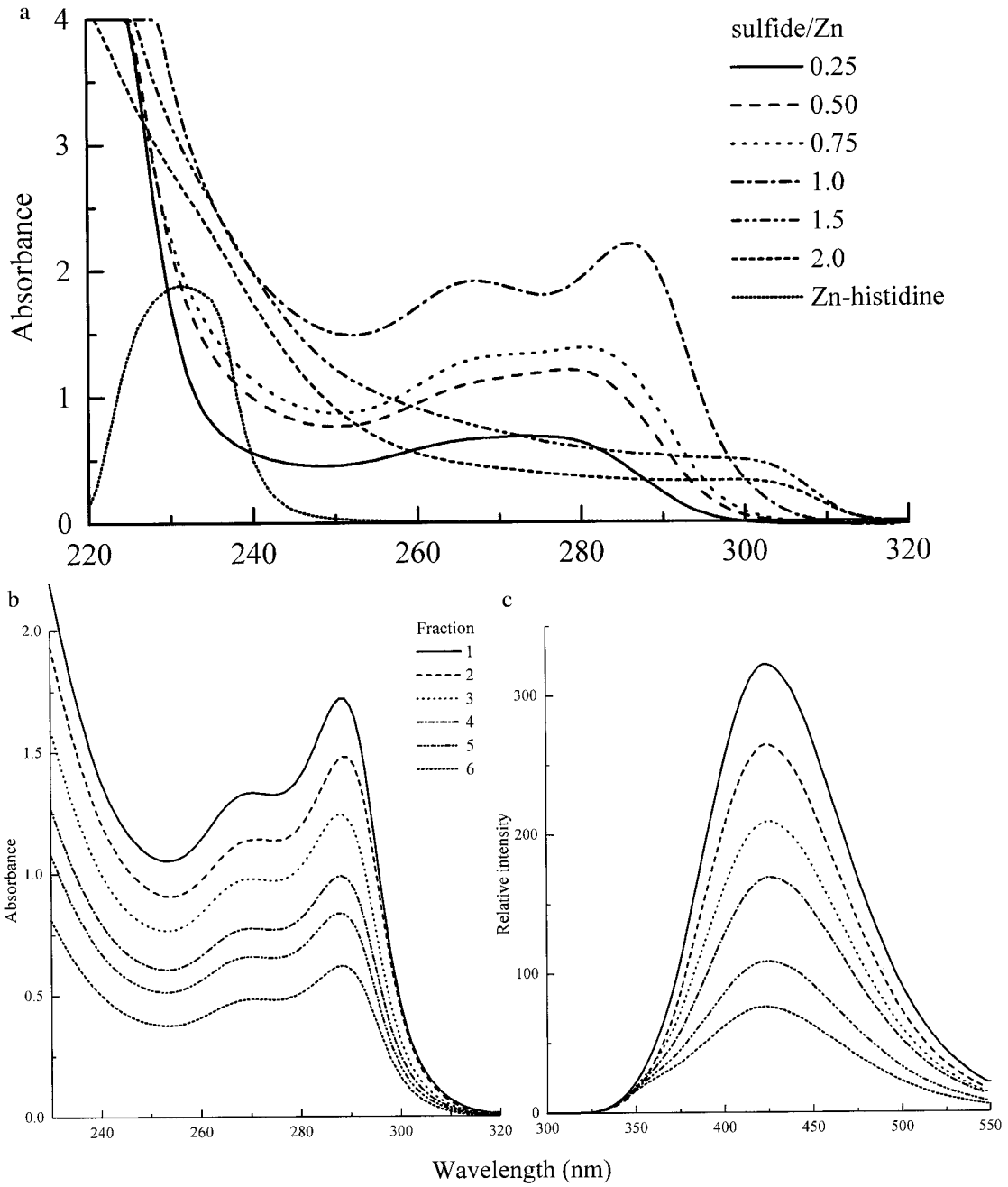

FIG. 1. Steady-state, room temperature optical spectra of histidine-ZnS NCs prepared in Tris. (a) UV/Vis absorption spectra showing the effects of increasing sulfide titrations into zinc-histidine complex. Spectra were obtained by diluting original samples to concentrations of about 20 μg Zn/mL. (b) UV/Vis spectra of 1.0 sulfide/Zn sample fractions obtained from a Sephadex G-25 column. Fraction numbers are arbitrary; Fraction 1 represents the peak fraction containing the highest concentration of histidine-ZnS (based on [zinc]). (c) Corresponding fluorescence spectra showing higher intensity and narrower peaks for samples with greater concentration of histidine-ZnS NCs.

ZnS NCs prepared via glutathione, phytochelatin, or cysteine matrices, and may yield better results in applications such as biolabeling or photocatalysis (13–15).

Electron microscopic characterization. To confirm that sulfide incorporation and NC formation was indeed responsible for the observed optical properties, hrTEM and SAED were performed on a representative sample of His-ZnS NCs prepared with 1.0 sulfide/Zn ratio. A high-resolution TEM micrograph and an electron diffraction pattern are shown in Fig. 2. The appearance of distinct lattice planes in the hrTEM image (3.0 ± 0.3 Å, lattice spacing) indicates a crystalline ZnS product (Fig. 2, left). The average nanocrystal size of a sample prepared with 1.0 sulfide/Zn ratio was deter-

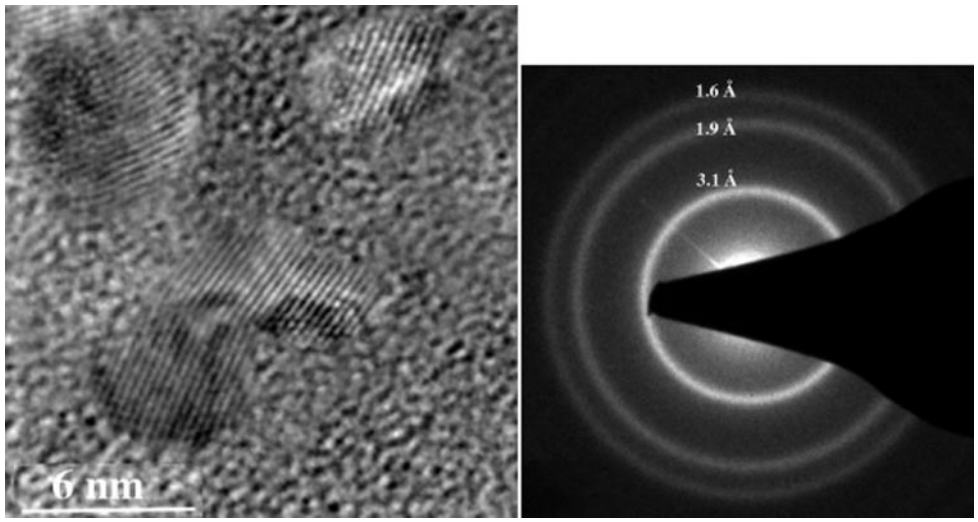

FIG. 2. (Left) High-resolution TEM image of a representative sample of histidine-capped ZnS nanocrystals (1.0 sulfide/Zn) showing resolved lattices. (Right) Selected area electron diffraction pattern of same sample. An intense diffraction ring at ~3.1Å, as well as diffractions at 1.9 Å and 1.6 Å are visible, corresponding to the (002), (110), and (112) planes of the hexagonal ZnS crystal, respectively (19).

mined to be 4.24 ± 0.66 nm. The SAED pattern (Fig. 2, right) displayed diffraction rings at 3.12 Å, 1.92 Å and 1.63 Å, corresponding to a hexagonal (wurtzite) crystal structure of ZnS (19).

Dual-peak absorption and enhanced fluorescence of histidine-ZnS NC populations. The bimodal absorption witnessed at intermediate sulfide/Zn ratios (Fig. 1a, 0.75 and 1.0 S/Zn) was hypothesized to be due either to multiple NC populations or the first and second excitonic transitions of a single NC population (18). Charge transfer between the histidine amino or carboxyl group and a charge vacancy at the ZnS NC surface was dismissed, as ZnS NCs prepared with histamine (lacks carboxyl) or imidazole (lacks amino and carboxyl) also showed dual-absorption peaks (data not shown). Meanwhile, the synthesis of histidine-ZnS NCs in water (adjusted to pH 11 with NaOH) also resulted in the dual absorption effect (Fig. 3a). However, a major difference between samples prepared in Tris and water (pH 11) was that the samples had a preference for either the ~260 nm or the ~290 nm peak depending on the buffer. The ~290 nm peak was favored in samples prepared with Tris, whereas the ~260 nm peak was favored for samples prepared with water (pH 11). The nature of this preference due to buffer effects is under investigation.

Size-exclusion chromatography was performed on a dual-peak sample prepared in water, this time using an apparatus with greater resolution (Sephadex G-50 matrix, thinner column and slower flow rate). The UV/Vis absorption spectra showed that the dual-peak absorption could be resolved by this method (Fig. 3b). Fractions 11–14 showed the ~290 nm peak, while fraction 22 showed a sharp ~260 nm peak. Compositional analyses by atomic absorption spectroscopy and methylene blue reduction assay (20) revealed that zinc and sulfide were present in these fractions at about 1:1 ratios as expected (data not shown) (13–15). The ability to separate the two absorption peaks via size-exclusion chromatography implies a reaction mechanism in which two populations are formed. Fluorescence excitation spectra (Fig. 3c) showed that the samples having the dual peak absorption also had dual-peak excitation maxima, further suggesting the formation of two NC populations. Corresponding fluorescence emission spectra are shown in Fig. 3d.

The greater than ten-fold fluorescence enhancement in histidine-ZnS NCs (Figs. 1c, 3d, and data not shown), as compared to cysteine-ZnS NCs, may be due to the imidazole moiety of histidine. Charge delocalization occurs within the imidazole ring, making it susceptible to excitation upon irradiation by light of sufficient energy. Subsequently, the photoexcited states may lead to charge transfer from the imidazole moiety to the ZnS native structure, enhancing fluorescence intensities (21). Alternatively, the histidine capping material may be more efficient in surface passivation than the GSH- or cysteine-chelators, therefore preventing deep trap surface states that can lead to nonradiative recombination (22).

Sulfide incorporation: Reaction mechanism. The following general mechanism for sulfide nucleation at zinc-histidine centers is proposed. Upon titration of sulfide into preformed zinc-histidine complexes, a competition for metal between the sulfide and histidine is introduced. This competition is governed by the stabilities of the subsequent complexes that may be formed, and is controlled primarily by the concentrations of the respective reagents. The zinc-histidine complex (at two-fold excess histidine) has a dissociation constant

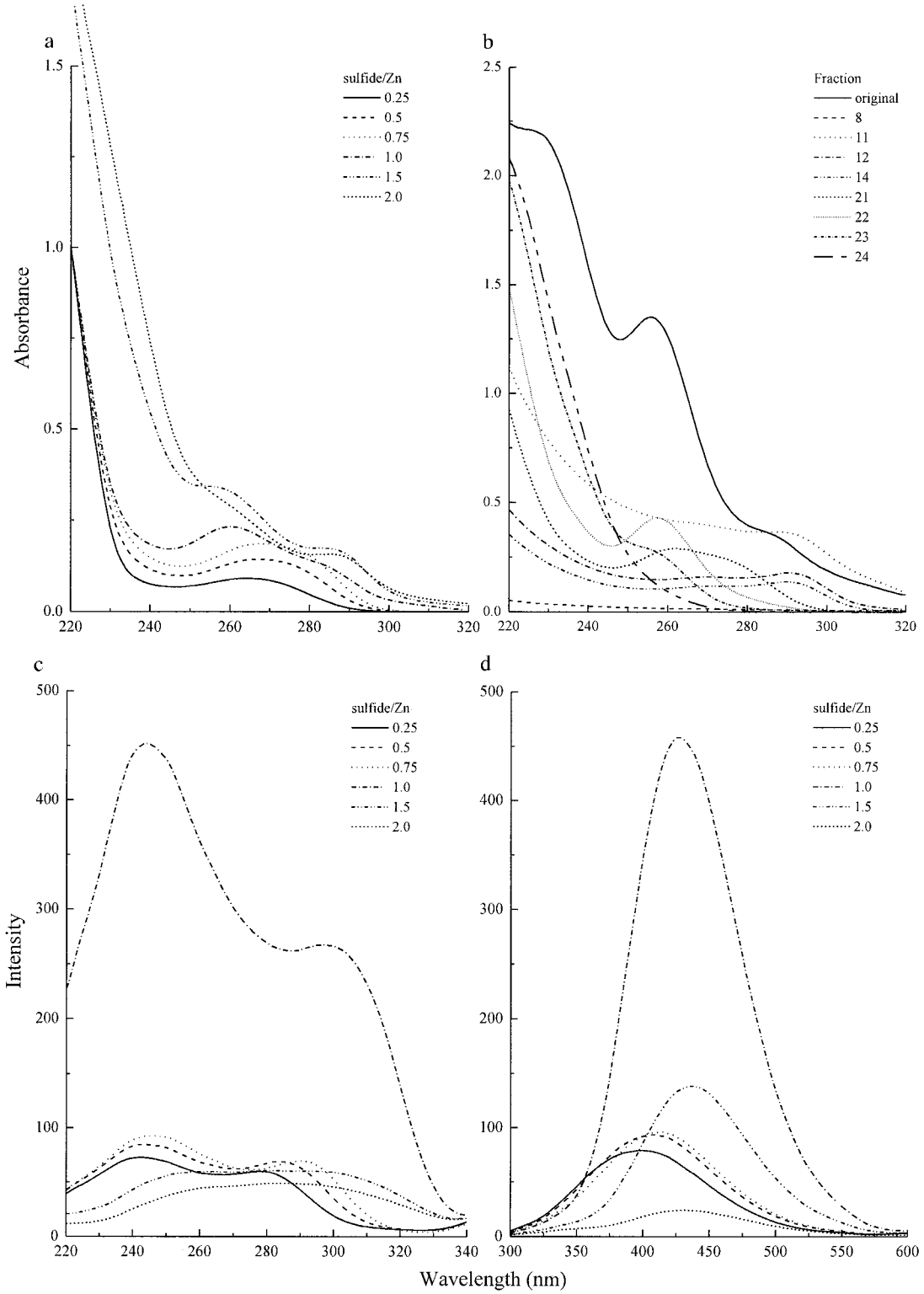

FIG. 3. Optical spectra of histidine-ZnS NCs prepared in water (pH 11). (a) UV/Vis absorption maxima shift to higher wavelengths with increasing sulfide/Zn ratio. Unlike samples prepared with Tris buffer, the samples with dual-peak absorption spectra show a preference for the lower wavelength peak (~260 nm). (b) Absorption spectra of 1.5 sulfide/Zn sample fractions eluting from a Sephadex G-50 column. "Original" refers to sample prior to size-fractionation. (c) Fluorescence excitation spectra of original samples (without size-fractionation) show dual-excitation maxima. (d) The corresponding fluorescence emission spectra (excited at 240 nm) show optimal intensity for 1.0 sulfide/Zn sample.

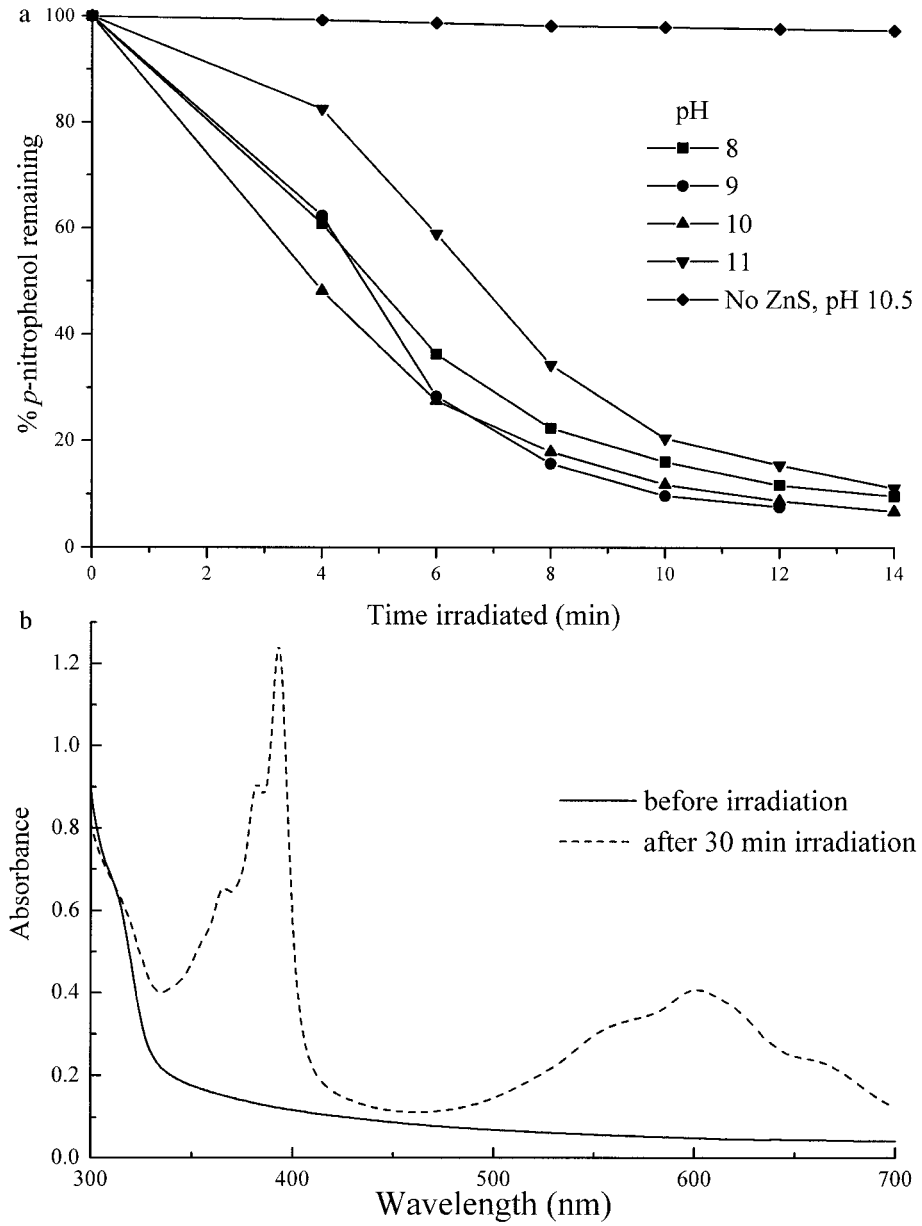

FIG. 4. Demonstration of photoredox reactions on histidine-ZnS NCs. (a) Photocatalytic, oxidative degradation of pNP in the presence of NCs prepared with 1.0 sulfide/Zn at varying pH. Degradation at pH 9 and 10 seemed to be most optimal under these reaction conditions. (b) UV/Vis absorption spectra of paraquat before and after irradiation in the presence of histidine-ZnS NCs. The appearance of absorbance maxima near 400 and 600 nm indicates reduction of paraquat.

(K_d, in water at 25°C) of 8.7×10^{-13} (23). Zinc-sulfide has greater stability, with a K_d value of 1.1×10^{-24} (24). Upon titration of sulfide, formation of histidine-capped ZnS progresses by displacement of histidine by sulfide at the zinc-histidine complex. By using appropriate amounts of the histidine and sulfide, the conditions described herein have been elucidated to allow efficient incorporation of sulfide into zinc-histidine complexes to form nanocrystals. Agglomeration of thus formed histidine-ZnS NCs into larger, bulk particles is prevented by the steric barrier introduced by the capping group as well as the net negative surface charge of the nanoparticles (20, 25).

Photo-redox reactions at the histidine-ZnS NC surface. An innovative application of semiconductors is in the photocatalytic degradation of environmental contaminants (26). By using smaller, nanocrystalline semiconductor particles such as these histidine-ZnS NCs, photocatalytic rates may be enhanced. The photochemistry on histidine-ZnS NCs leading to oxidative and reductive degradation of *p*-nitrophenol (pNP) and

paraquat, respectively, are shown in Figs. 4a and 4b. The photocatalytic degradation of pNP was shown to occur at all tested pH values (Fig. 4a), although too high a pH had lower rates due presumably to hydroxyl radical self-quenching (15). In the presence of NCs, near-complete decolorization of pNP was observed after 14 min of irradiation with the UV light source. The control reaction (pH 10.5), which lacked histidine-ZnS NCs, did not show significant loss of pNP at 14 minutes of irradiation.

The reduction of paraquat in the presence of His-ZnS NCs was observed after 30 minutes of irradiation with the shortwave UV lamp (Fig. 4b). The appearance of absorption shoulders at 395 nm and near 600 nm indicates reduction of paraquat (13). The absorption spectrum of paraquat irradiated without His-ZnS NCs did not change. These laboratory-scale experiments demonstrate the potential applicability of these NCs in degradation of environmental pollutants.

SUMMARY

Zinc-histidine complexes were shown to be efficient nuclei for incorporation of sulfide. The optical properties were akin to ZnS semiconductor nanocrystals (NCs). Electron microscopic analyses confirmed their nanocrystalline nature and revealed a hexagonal ZnS structure. Size-exclusion chromatography techniques, in combination with optical spectra, suggested the formation of multiple thermodynamically favored ZnS NC species at intermediate sulfide concentrations. Photocatalytic degradation of model pollutants (*p*-nitrophenol and paraquat) demonstrated the potential applicability of these histidine-ZnS NCs in photocatalysis applications.

ACKNOWLEDGMENTS

We thank Dr. Weon Bae and members of our laboratory for critical comments and discussion on NCs. Financial support from CULAR, UCR Academic Senate and ENTX Graduate Program is gratefully acknowledged.

REFERENCES

1. Goldberger, R. F., and Kovach, J. S. (1972) Regulation of histidine biosynthesis in *Salmonella typhimurium*. *Curr. Top. Cell. Regulation.* **5,** 285–308.
2. Boldyrev, A., and Abe, H. (1999) Metabolic transformation of neuropeptide carnosine modifies its biological activity. *Cell. Mol. Neurobiol.* **19,** 163–175.
3. Voet, D., and Voet, J. G. (1995) Biochemistry, Wiley, New York.
4. Takatsuji, H. (1999) Zinc-finger proteins: The classical zinc finger emerges in contemporary plant science. *Plant Mol. Biol.* **39,** 1073–1078.
5. Green, A., Parker, M., Conte, D., and Sarkar, B. (1998) Zinc finger proteins: A bridge between transition metals and gene regulation. *J. Trace Elem. Exp. Med.* **11,** 103–118.
6. Krämer, U., Cotter-Howells, J. D., Charnock, J. M., Baker, A. J. M., and Smith, J. A. C. (1996) Free histidine as a metal chelator in plants that accumulate nickel. *Nature* **379,** 635–638.
7. Salt, D. E., Prince, R. C., Baker, A. J. M., Raskin, I., and Pickering, I. J. (1999) Zinc ligands in the metal hyperaccumulator *Thlaspi caerulescens* as determined using X-ray absorption spectroscopy. *Environ. Sci. Technol.* **33,** 713–717.
8. Lasat, M. M., Pence, N. S., Garvin, D. F., Ebbs, S. D., and Kochian, L. V. (2000) Molecular physiology of zinc transport in the Zn hyperaccumulator *Thlaspi caerulescens*. *J. Exp. Bot.* **51,** 71–79.
9. Mehra, R. K., and Winge, D. R. (1991) Metal ion resistance in fungi: Molecular mechanisms and their regulated expression. *J. Cell. Biochem.* **45,** 30–40.
10. Dameron, C. T., Reese, R. N., Mehra, R. K., Kortan, A. R., Carroll, P. J., Steigerwald, M. L., Brus, L. E., and Winge, D. R. (1989) Biosynthesis of cadmium sulfide quantum semiconductor crystallites. *Nature* **338,** 596–597.
11. Dameron, C. T., Smith, B. R., and Winge, D. R. (1989) Glutathione-coated cadmium sulfide crystallites in *Candida glabrata*. *J. Biol. Chem.* **264,** 17355–17360.
12. Mehra, R. K., Mulchandani, P., and Hunter, T. C. (1994) Role of CdS quantum crystallites in cadmium resistance in *Candida glabrata*. *Biochem. Biophys. Res. Commun.* **200,** 1193–1200.
13. Bae, W., and Mehra, R. K. (1998) Properties of glutathione- and phytochelatin-capped CdS bionanocrystallites. *J. Inorg. Biochem.* **69,** 33–43.
14. Bae, W. O., Abdullah, R., Henderson, D., and Mehra, R. K. (1997) Characteristics of glutathione-capped ZnS nanocrystallites. *Biochem. Biophys. Res. Commun.* **237,** 16–23.
15. Torres-Martínez, C. L., Nguyen, L., Kho, R., Bae, W., Bozhilov, K., Klimov, V., and Mehra, R. K. (1999) Biomolecularly capped uniformly sized nanocrystalline materials: Glutathione-capped ZnS nanocrystals. *Nanotechnology.* **10,** 340–354.
16. Nguyen, L., Kho, R., Bae, W., and Mehra, R. K. (1999) Glutathione as a matrix for the synthesis of CdS nanocrystallites. *Chemosphere.* **38,** 155–173.
17. Bruchez, M., Jr., Moronne, M., Gin, P., Weiss, S., and Alivisatos, A. P. (1998) Semiconductor nanocrystals and fluorescent biological labels. *Science* **281,** 2013–2016.
18. Henglein, A. (1989) Small-particle research—Physicochemical properties of extremely small colloidal metal and semiconductor particles. *Chem. Rev.* **89,** 1861–1873.
19. Powder Diffraction File: Alphabetical Index, Inorganic Phases (1985) JCPDS International Center for Diffraction Data, USA.
20. King, T. E., and Morris, R. O. (1967) Determination of acid-labile sulfide and sulfhydryl groups. *Methods Enzymol.* **10,** 634–637.
21. Bringuier, E. (1994) Native anatomy of ZnS-type electroluminescence. *Appl. Phys.* **75,** 4291–4312.
22. Nirmal, M., and Brus, L. (1999) Luminescence photophysics in semiconductor nanocrystals. *Acc. Chem. Res.* **32,** 407–414.
23. Martell, A. E., and Smith, R. M. (1982) Critical Stability Constants, Plenum Press, New York.
24. Freier, R. K. (1976) Aqueous Solutions: Data for Inorganic and Organic Compounds, Walter de Gruyter, Berlin.
25. Murray, C. B., Norris, D. J., and Bawendi, M. G. (1993) Synthesis and characterization of nearly monodisperse CdE (E = S, Se, Te) semiconductor nanocrystallites. *J. Am. Chem. Soc.* **115,** 8706–8715.
26. Ollis, D. F., Pelizzetti, E., and Serpone, N. (1991) Photocatalyzed destruction of water contaminants. *Environ. Sci. Technol.* **25,** 1522–1529.